Articles in PresS. J Neurophysiol (October 10, 2012). doi:10.1152/jn.00502.2012

1

Title:	A mathematical model of dopamine autoreceptors and uptake inhibitors and their influence on tonic and phasic dopamine signaling
Running head:	Uptake and autoreceptors influence DA signals
Authors:	**Name** / **Address** Jakob Kisbye Dreyer — Department for Neuroscience and pharmacology, University of Copenhagen, 2200 Copenhagen, Denmark. Jørn Hounsgaard — Same as 1st
Corresponding Author	Jakob Kisbye Dreyer Department for Neuroscience and pharmacology University of Copenhagen Blegdamsvej 3, 12.5 2200 Copenhagen Denmark. Email: jakobdr@sund.ku.dk Telephone: +45 35327553 (work) / +45 60809551 (mobile)
Author contributions	JKD: Developed and designed the model, designed study, analyzed data, wrote the paper JDH: analyzed data, wrote the paper

2

Abstract:

Dopamine (DA) D2-like autoreceptors are an important component in the DA system. But their influence on postsynaptic DA signaling is not well understood. They are, directly or indirectly, involved in drug abuse and in treatment of schizophrenia and attention deficit hyperactive disorder: DA autoreceptors influence the behavioral effect of cocaine and methylphenidate and may be the target of antipsychotic medication such as haloperidol. DA autoreceptors are active at two levels: Somatodendritic autoreceptors mainly influence firing rate of DA neurons and presynaptic autoreceptors control release of neurotransmitter at axonal terminals. Here we develop a mathematical model that captures the dynamics of this dual autoregulation system. Our model predicts a biphasic autoreceptor response between DA terminals and somatodendritic regions that influences the postsynaptic integration of DAergic firing patterns. We applied our model to study how DA uptake inhibition affects the translation of DA cell firing into activation of post synaptic DA receptors. While uptake inhibition increased tonic activation of low affinity postsynaptic receptors, high affinity state receptors saturated and thus became insensitive to phasic DA signaling. This effect had remarkable regional specificity: While high affinity DA receptors in nucleus accumbens saturated at low levels of uptake inhibition they only saturated at higher levels of uptake inhibition in dorsal striatum. Based on high affinity receptor saturation, the model predicted that removal of autoreceptor control would lead to cocaine hypersensitivity.

Keywords

Burst, striatum, nucleus accumbens, D2 receptor, D1 receptor, cocaine, methylphenidate, D2 antagonist, D2 agonist, locomotor, ADHD, reward, antipsychotic, modeling, computational

Introduction

Dopamine (DA) in nucleus accumbens and dorsal striatum is critical for reward and goal oriented behavior (Grace et al. 2007; Schultz 1998). DA signaling, or the lack thereof, is the turning point of major disorders such as drug abuse, schizophrenia, Parkinson's Disease, and attention deficit hyperactive disorder (ADHD) (Dagher and Robbins 2009; Howes and Kapur 2009; Volkow et al. 2010).

A wide range of DA related behavior and cognitive functions are distorted by either too low or too high DA levels (Cools and D'Esposito 2011). Thus precise control over the DA signal seems highly critical to normal function. For this reason it is no surprise that DA neurons are controlled by a complex system of D2 and D3 autoreceptors. Reduced autoreceptor control has been implicated in impulsivity (Buckholtz et al. 2010) and enhances the behavioral effect of cocaine (Bello et al. 2011). DA autoreceptors may even be primary target of certain antipsychotics (Moller 2005).

DA autoreceptors affect multiple aspects of DA signaling including firing rate, DA synthesis and terminal release (Beaulieu and Gainetdinov 2011). DA release in somatodendritic regions interacts with somatodendritic autoreceptors inhibiting firing of DA neurons (Beckstead et al. 2004; Cragg and Greenfield 1997; Pucak and Grace 1994). At the same time DA release from axonal terminals interacts with D2 receptors expressed on presynaptic terminals regulating release and synthesis (Benoit-Marand et al. 2001; Dugast et al. 1997; el Mestikawy et al. 1986; Schmitz et al. 2003).

The rich dynamics of DA autoreceptors and their influence on DA levels and transients has been studied intensively (Benoit-Marand et al. 2001; Gonon and Buda 1985; Phillips et al. 2002; Zhang et al. 2009). However, a unified description of the coupling between pre- and postsynaptic DA signaling is still lacking. Fixed amplitude models neglect dynamic changes in DA release (Dreyer et al. 2010; Venton et al. 2003; Wightman and Zimmerman 1990). Consequently, they are only valid for small perturbations in DA signaling. Variable release models include facilitation and depression of release by artificially evoked spike trains (Montague et al. 2004). However, the static parameters of the variable release model include implicit effects of multiple factors including autoreceptors, uptake, diffusion, and tonic DA activity. Thus the dynamic changes in DA signaling when their relative contributions are altered by drugs or disease are not accounted for.

Here we model how somatodendritic and presynaptic autoreceptors influence activation of post synaptic DA D1 and D2 receptors by DA cell firing. In our model, the contribution of autoreceptors is explicit so that effects of their manipulations can be estimated and tested. Reliable estimates of concurrent pre- and postsynaptic DA transmission required a bottom-up biophysical reconstruction of DA release in axonal terminal fields, including estimates of the occupancy of terminal autoreceptors. At the same time concurrent somatodendritic release was simulated to provide negative feedback for the firing of DA neurons.

In the first part of this report we provide estimates of DA levels and transients and make predictions on how these may be altered in typical experimental paradigms

where DA release is evoked by electrical stimulations. We found that autoreceptors introduce an interplay between somatodendritic and terminal DA.

We then investigate how autoreceptors influence postsynaptic signaling of naturally occurring phasic firing patterns relevant for reward signaling (Schultz 1998). We found that high and low affinity postsynaptic receptors were differentially affected by bursts and pauses in DA cell firing. Autoreceptors effectively increased the specificity of burst and pauses to low and high affinity post synaptic receptors.

Finally, we apply the model to study the effect of dopamine uptake inhibition on the translation of DA cell firing to activation of postsynaptic receptors. Here, the most prominent effect of uptake inhibition was saturation of high affinity post synaptic receptors. This blocked their ability to respond to phasic DA cell firing. In nucleus accumbens this occurred at levels of uptake inhibition in the therapeutic range whereas dorsal striatum was affected by uptake inhibition at locomotor stimulating levels.

Glossary

ADHD	Attention Deficit Hyperactive Disorder
$AR(\mathbf{r},t)$	Occupancy at time t of autoreceptors at location $\mathbf{r}$

$AR_j^i(t)$	Average occupancy autoreceptors at terminal i on neuron j
AUC	Area under curve
C	Concentration of DA
DA	Dopamine
DAT	Dopamine transporter
ΔC_{soma}	Incremental release of somatodendritic DA for a single action potential
D_{coc}^{ip}	Dose of ip cocaine in mg/kg
D_{coc}^{iv}	Dose of iv cocaine in mg/kg
DRH	High affinity postsynaptic dopamine receptor (EC50 = 0.010 µM)
DRL	Low affinity postsynaptic dopamine receptor (EC50 = 1 µM)
DS	Dorsal striatum
i.p.	Intra peritoneal
i.v.	Intra veneous
k_{off}	Off-rate for DA binding to presynaptic autoreceptors
k_{on}	On-rate for DA binding to presynaptic autoreceptors
K_{app}	Apparent Michaelis Menten constant
K_i	Inhibition constant for competive uptake inhibitor
K_m	Michaelis Menten constant
MP	Methylphenidate

NAcc	Nucleus accumbens
v_{eff}	Effective firing rate of DA neurons, realized by input firing rate minus inhibition by somatodendritic autoreceptors
v_{in}	Input firing rate to the model. The firing rate realized in absence of somatodendritic autoinhibition
$P_{\max}$	Highest possible vesicular release probability
$P_{\min}$	Lowest possible vesicular release probability
P_r	Vesicular release probability
SNc	Substantia nigra pars compacta
$V_{\max}$	Michaelis Menten uptake parameter
VTA	Ventral tegmental area

Methods

The aim of this work was to develop an integrated model of DA volume transmission that can predict the dynamic effects of somatodendritic and presynaptic DA autoreceptors and how these influence the postsynaptic effect of DA cell firing. The input parameters to the model are primarily based on observations in rodents.

We analyzed DA signaling from a systems perspective and investigated volume mediated signals by an ensemble of DA neurons projecting to a common target area in NAcc or DS (Dreyer et al. 2010). We assumed that the activity of the ensemble was described by the population averaged firing rate. The experimentally observed firing rate is determined by a combination of external synaptic input and intrinsic currents

where inhibitory GIRK channels controlled by somatodendritic autoreceptors play a partial role. In our systems approach we separated these terms so that

$$\nu_{eff} = \nu_{in} - \Delta\nu_{auto}$$

Equation 1

Here ν_{eff} is the *effective firing rate* and ν_{in} is the *input firing rate*. The effective firing rate is the firing rate observed experimentally and determines both somatodendritic and terminal release. The input firing rate is defined as the firing rate of DA neurons driven by all external and internal current inputs *except* those mediated by autoreceptors. The last term, $\Delta\nu_{auto}$, is the reduction in firing rate mediated by currents induced by somatodendritic autoinhibition.

To keep matters simple we avoided direct calculation of the ionic currents assumed to be responsible for these terms. Instead, we established an empirical relation between DA levels in the somatodendritic region directly and the effective firing rate based on experimental data (See Figure 1 and Equation 5).

Similarly we assumed terminal release probability to be regulated by the occupancy of presynaptic autoreceptors. These autoreceptors are assumed to be sensitive to the local DA level around release sites. Again we established a heuristic relation between occupancy of presynaptic autoreceptors at a given terminal and its release probability but avoid direct calculation of the underlying ionic currents at the terminal assumed to mediate the effect.

Consequently, the dual autoregulation system was modeled as two systems, somatodendritic and terminal, each providing a feedback mechanism based on the

local DA concentration. Finally, activation of post synaptic DA receptors was predicted from the spatiotemporal concentration extracellular DA in terminal areas assuming DA volume transmission (Dreyer et al. 2010). When applying the model to investigate the effect of uptake inhibition we assumed that these directly increased the apparent Michaelis Menten constant of the uptake.

Implementation of competitive uptake inhibition

When simulating inhibited uptake conditions we used an apparent Michaelis-Menten constant K_{app} where $K_{app} \geq K_M$, where K_M = 0.16 µM is the native uptake constant (John and Jones 2007). To bridge with in vivo studies, we assumed the following linear relation between i.p. dose of cocaine and apparent uptake constant

$$K_{app} = 0.056\mu\mathrm{M}\,(\mathrm{mg/kg})^{-1} D_{coc}^{ip} + K_M$$

Equation 2

where D_{coc}^{ip} is the i.p. dose of cocaine in mg/kg. Equation 2 is based on the observation by Oleson et al (Oleson et al. 2009) that K_{app} peaks at 1.0062 µM following administration of 15 mg/kg i.p. cocaine. Note that for this value of K_{app} is reached 20 minutes after delivery of drug (Oleson et al. 2009). We also use Equation 2 when discussing uptake inhibited by i.p. methylphenidate (MP). In this case we correct for the different inhibitory potency at the DAT (K_I = 0.35 µM for cocaine and K_I = 0.21 µM for methylphenidate (John and Jones 2007)). Relative scales between K_{app} and doses of i.p. cocaine and i.p. MP are provided under the *x*-axis of Figure 1A. Under these assumptions, 2 mg/kg i.p. MP or 3 mg/kg i.p. cocaine blocks

approximately 50% of the DA transporters and we consider this to be the therapeutically relevant level of DAT inhibition (Volkow et al. 1998).

In order to estimate apparent uptake constants following i.v. cocaine. Here we interpolated linearly over the peak values in experimentally observed K_{app} by España et al (Espana et al. 2008). The resulting relation was

$$K_{app} = 0.80\ \mu\mathrm{M}\,(\mathrm{mg/kg})^{-1} D_{coc}^{iv} + K_M$$

Equation 3

Note that for iv administration the peak value occurs within 30-60s after delivery of drug (Espana et al. 2008).

Our simulations assume steady state concentrations of inhibitor on a time scale of 1 minute which approximate i.p. administration better than i.v. adminstration. We will therefore use Equation 2 except where noted.

Since we assume constant levels of uptake inhibitor our results are mostly relevant for therapeutic applications, where methylphenidate is a typical drug. However many animal studies use i.p. cocaine as model substance. Therefore we will compare our computational results with empirical results of either cocaine or methylphenidate where appropriate.

Determination of effective DAergic firing rate and somatodendritic DA concentration

The effective firing rate is determined from the input firing rate and somatodendritic autoinhibition depending on the somatodendritic DA concentration.

Thus we needed to calculate somatodendritic DA levels in our model. Experimentally the spike-amplitude of DA release in somatodendritic regions is modulated very little by autoreceptors (Cragg and Greenfield 1997). For simplicity we therefore used a fixed amplitude model to calculate the somatodendritic DA level as function of the effective firing rate (Wightman and Zimmerman 1990). The somatodendritic DA concentration, *C*, was determined numerically by solving

$$\frac{dC_{soma}}{dt} = \Delta C_{soma}\ \Pi_{spike}(\nu_{eff}) - \frac{V_{\max}^{soma} C_{soma}}{K_{app} + C_{soma}}$$

Equation 4

where ΔC_{soma} = 0.02 µM is the incremental release of DA pr spike, $V_{\max}^{soma}$ = 0.2µM/s is the maximum DA uptake capacity in the somatodendritic region (John et al. 2006), and Π_{spike} is a stochastic variable taking value 1 if a spike occurs within the current time step of the integration and 0 otherwise. This was determined by a Poisson process depending on the effective firing rate ν_{eff}. To minimize the effect random fluctuations we averaged Equation 4 10 times to calculate C_{soma}.

To model somatodendritic autoreceptors we needed to determine the link between somatodendritic DA levels and how this reduce effective firing rate. For this we used the relation between tonic firing rate and iv dose of cocaine established by Einhorn et al (Einhorn et al. 1988). We first assumed that ν_{eff} = 4 Hz in the control case and linked effective firing rate and K_{app} calculated using Equation 3 (Figure 1A, each data point corresponds to an observation by Einhorn et al. Filled markers indicate conditions shown in Panel B). We then used Equation 4 to calculate somatic DA levels for each pair of ν_{eff} and K_{app} (Figure 1B). We then observed a linear relation

between the average DA levels and effective firing rate (Figure 1C, circles are constructed from Einhorn observations, filled markers are the conditions shown in Figure 1B, dashed line is the linear relation $\nu_{\text{eff}} = 5\text{ Hz} - 8\text{ Hz}/\mu\text{M} * C_{\text{soma}}$).

We assumed this linear relationship to reflect a fundamental relation between different components affecting firing of DA neurons. We therefore generalized the linear relation and assumed that autoreceptors reduce cell firing with an amount proportional to somatodendritic DA levels.

Since effective firing rate determines its own inhibition we constantly updated effective firing rate and somatodendritic DA levels in parallel. In each time step ν_{eff} was determined from the instantaneous somatodendritic DA levels using

$$\nu_{eff}(t) = \begin{cases} \nu_{\text{target}}(t) - \alpha C(t) & \text{for } \alpha C(t) < \nu_{\text{target}}(t) \\ 0 & \text{for } \alpha C(t) \geq \nu_{\text{target}}(t) \end{cases} \quad \text{Equation 5}$$

where α=8 Hz/μM and where ν_{in} indicates the input firing rate. Note that if $\alpha C_{\text{soma}} > \nu_{\text{in}}$, the effective firing rate is set to 0. We use ν_{in} as control parameter of the model and bursts and pauses in neuron population are generated by temporal variations in input firing rate.

When simulating artificially evoked release we assumed that the firing rate of the evoked spike train was independent on somatodendritic autoinhibition.

Calculation of extracellular DA level in axon terminal regions

The DA levels in terminal regions were calculated by a diffusion model incorporating DA vesicular release from distinct release sites, extracellular diffusion and Michaelis Menten reuptake. Details and parameters are described in Dreyer et al (Dreyer et al. 2010). In brief, the model describes 3D spatiotemporal evolution of DA

concentration in cubic volume. DA levels in the simulation space were determined by vesicular release from spatially distinct terminals.

By selecting different parameter settings we modeled DA signaling in either Nucleus accumbens (NAcc) or dorsal striatum (DS). In our model these two areas differ by innervation density of DA terminals (DS, 0.1 terminals pr μm^3; NAcc, 0.06 terminals pr μm^3 (Doucet et al. 1986) and by total uptake capacity (DS, Vmax = 4.1 μMs^{-1} ; NAcc, , Vmax = 1.5 μMs^{-1})(Cragg and Rice 2004; Garris et al. 1994a). The size of the simulation space was set to accommodate exactly 1500 DA release sites. Thus the diameter of the simulation space was 29.2 μm when simulating NAcc and 24.7 μm when simulating DS. Figure 2A shows a high spatial resolution image of instantaneous DA concentrations during tonic firing. Black dots indicate DA release sites and the spatial concentration of extracellular DA is indicated by color.

Due to anatomical constraints, the terminal simulation space is assumed to contain terminals from an ensemble of 100 different neurons. Spikes of each neuron were determined by independent Poisson processes with intensity determined by ν_{eff}. Thus the average firing rate across the ensemble was approximately ν_{eff} but with fluctuations due to the random spike generating process. The Poisson process was also used when simulating evoked release.

In order to accurately model the location of DA transporters at terminals, we focused DA uptake at the release sites (Figure 2B, spatial resolution as in typical simulations). Details concerning the implementation of localized DA uptake are given below.

Autoreceptor control of terminal release probability

Experimental voltammetry studies show that autoreceptor control of axonal terminal DA release is bidirectional: Release is increased by D2 antagonist drugs and decreased by D2 agonists. Typically the dynamic range observed roughly covers a factor of 2 to either side in evoked DA release (Dugast et al. 1997; Gonon and Buda 1985; Herr et al. 2010; Wu et al. 2002). In our model, the spike amplitude of terminal DA release is proportional to the density of release sites, the number DA molecules in DA vesicles, and the probability that a terminal releases a vesicle with an action potential (Dreyer et al. 2010; Wallace and Hughes 2008). Even though DA autoreceptors could potentially be involved in regulation a all of these factors, we find it most likely that the fast time scale effects relevant for phasic DA signaling are mediated by dynamic modulation of the release probability.

In our model terminal *i* on neuron *j* release a vesicle with probability P_j^i

when neuron *j* fires. In a preliminary study we estimated the typical vesicular release probability to be 6% (Dreyer et al. 2010). To be consistent with the approximately 2-fold dynamic range of release amplitudes we therefore set Pmin= 2.5 % as the minimal release probability, corresponding to terminal autoreceptors fully activated, and Pmax = 15% as the maximal release probability, realized when terminal autoreceptors are fully deactivated. To enable bidirectional control we assumed the EC50 of terminal autoreceptors to be 40 nM, around the expected basal level of the model (Dreyer et al. 2010).

Occupancy and spatial distribution of presynaptic autoreceptors

We assumed that the release probability pr action potential for each release site was controlled by autoreceptors sensitive to the time varying DA level around the terminal. The occupancy of autoreceptors at location **r** at time *t* was calculated dynamically by numerical integration of

$$\frac{d\,\mathrm{AR}(\mathbf{r},t)}{dt} = C(\mathbf{r},t)k_{on}\left(1-\mathrm{AR}(\mathbf{r},t)\right) - k_{off}\,\mathrm{AR}(\mathbf{r},t)$$

Equation 6

where *C(**r**,t)* is the concentration of DA at position **r** and at time *t,* AR(**r**,*t*) is the corresponding occupancy of autoreceptors and k_{off} and k_{on} denote the off and on rates of DA interaction with terminal D2 receptors. To our knowledge, these on-and off rates have not been directly measured for DA. We used k_{on} = 10 $\mu M^{-1}s^{-1}$ (Chance 1943) and set k_{off} = 0.4 s^{-1} to give 50% occupancy at the EC50 described above. We verified that the time course of autoinhibition was in agreement with experimental observations (Benoit-Marand et al. 2001; Phillips et al. 2002).

Equation 6 describes the occupancy state of autoreceptors at any location in simulation space. The influence of autoreceptors on a particular terminal was determined as a weighted average of AR(**r**, *t*) where autoreceptors close to the terminal have the highest influence. Thus for terminal *i* on neuron *j* the average occupancy of terminal autoreceptors at time *t* was determined by as

$$AR_i^j(t) = \int_{\Omega} \frac{AR(\mathbf{r},t)}{\left(2\pi r_{term}^2\right)^{3/2}} \exp\left(\frac{\left(\mathbf{r}-\mathbf{r}_{ij}\right)^2}{2r_{term}^2} \right) d\mathbf{r}$$

Equation 7

where r_{term} = 0.25 µm is the half width of the terminal (Pickel et al. 1992) and $\mathbf{r}_{ij}$ is the location of the terminal. The integral extends over the simulation space and the normalization was corrected for boundary effects.

Once the average occupancy of terminal autoreceptors for the terminal was established, the release probability was determined by linear interpolation

$$P_i^j(t) = \left(P_{\min} - P_{\max}\right) AR_i^j(t) + P_{\max}$$

Equation 8

where P_{min} = 2.5% and P_{max} = 15% as described above (Figure 2 C shows relationship between equilibrium DA concentration and P_r). Note that the release probability describes the probability of release for a single terminal, number *i* on neuron *j*. Different terminals in the simulation space will generally experience different dynamical DA concentrations and therefore have different release probability. In particular, a single vesicular release event will brifly reduce the release probability of the releasing terminal in a time span after the release (Figure 2 D, see red line at T = 2.2 s and blue line at T = 4.3 s).

Presynaptic location of dopamine transporters

Since DA transporters are primarily expressed on DA neurons near release sites (Hersch et al. 1997) we used a space dependent uptake,

293 $$V_{\max}(\mathbf{r}) = \sum_{ij} \frac{V_0}{\left(2\pi r_{term}^2\right)^{3/2}} \exp\left(\frac{\left(\mathbf{r}-\mathbf{r}_{ij}\right)^2}{2r_{term}^2}\right)$$

294 Equation 9

295 where V_0 is a constant equivalent to the uptake capacity pr terminal, other
296 parameters are defined as in Equation 7. The value of V_0 was selected so that the
297 total volume-averaged uptake was equal $V_{\max}$ in the simulation space, such as 1.5
298 µM/s for simulation of NAcc. In Equation 9 the uptake capacity is high near release
299 sites and low further away as shown in Figure 2B.

300 Electrochemical measurements of DA uptake typically use carbon about 50 µm long
301 (Venton et al. 2003). Such electrodes sample volumes considerably larger than 1 μm^3
302 and therefore report the volume average of $V_{\max}(\mathbf{r})$. In our simulations the DA levels
303 and activation of pre- and post synaptic receptors was also mainly determined by
304 the volume averaged uptake (see below).

305 1.1 Quantification of post synaptic DA signaling.

306 Post synaptic DA receptors are classified into D1-like and D2 like receptors
307 depending on their ability to facilitate or depress the production of post synaptic
308 cyclic AMP (Beaulieu and Gainetdinov 2011). Both of these receptor subtypes may
309 exist in high and low affinity states. We hypothesized spatially uniform distributions
310 of low affinity (DRL, EC50 ≈ 1000 nM) and high affinity (DRH, EC50 ≈ 10 nM)
311 receptors (May 1992) and assumed these receptors to be sensitive to DA volume
312 transmission in terminal areas. In each time step of the simulation, the activity of
313 post synaptic DA receptors was determined as a 3D volume integral of the spatial

distribution of terminal DA (Figure 2A) assuming local quasi-equilibrium (Dreyer et al. 2010).

The effect of bursts or pauses was quantified in terms the change in area under curve (ΔAUC), calculated as

$$\Delta\mathrm{AUC} = \int_0^T \left(DR_{phasic}(t) - \left\langle DR_{tonic} \right\rangle \right) dt$$

Equation 10

where $DR_{\mathrm{phasic}}(t)$ is the estimated activation of DA receptor (either high or low affinity) and $\left\langle DR_{tonic} \right\rangle$ is the average activation by tonic firing in the same brain region and with the same level of uptake inhibition. Except where stated, the integral extended over the whole duration of the transient, including possible long-term compensatory effects of somatodendritic and terminal autoinhibition. Note that when the phasic signal is a pause, the ΔAUC becomes negative.

Bursts and pauses were simulated as a repeating pattern of 4 cycles each with a period of 10 s simulated time. The initial DA level in the simulation space was estimated by the tonic firing rate, uptake and autoinhibition. To stabilize DA levels, simulations were run for 5s simulated time before collecting results.

The model was implemented in Matlab 7.8 (The Mathworks) and numerical integration was performed using the forward Euler method.

Results

Tonic and phasic activation of terminal autoreceptors

We used our model to investigate DA signaling in DS and NAcc, areas highly innervated by DA terminals.

We first investigated DA levels produced by steady state tonic firing. By setting ν_{in} = 5 Hz, our model stabilized at approximately 4 Hz effective firing rate and with constant somatodendritic DA level around 0.1 μM.

The tonic activity gave 0.047 $\pm$ 0.01 μM baseline level in DS and 0.067 $\pm$ 0.01 μM in NAcc (mean $\pm$ standard deviation). Here the standard deviation indicates variability due to random fluctuation in firing rate and stochastic release. Considering that critical parameters such as tonic firing rate, DA innervation density, and uptake have high variability even within same subject, we consider the above difference in tonic DA levels between NAcc and DS to be relatively small compared to the inherent uncertainty in our model (Garris et al. 1994b; Grace and Bunney 1984b; Hyland et al. 2002; Koulchitsky et al. 2012; Moquin and Michael 2009; Wightman et al. 2007).

With tonic activity, the average release probability across terminals was 7-8% (Figure 2D black line). Comparing with the maximal release probability (P_{max} = 15%) this relative difference indicates a substantial tonic occupancy of terminal autoreceptors as observed by Dugast et al (Dugast et al. 1997). In comparison, the

difference between input firing rate (5 Hz) and effective firing rate (4 Hz) mediated by tonic DA levels in somatodendritic regions was relatively small. This is in agreement with the 20% increase in firing rate after administration of D2 receptor antagonists observed by Pucak and Grace (Pucak and Grace 1994).

We then investigated the time course of autoinhibition using evoked transients. Here we simulated two evoked DA transients each generated by evoked release equivalent to 3 spikes at 100 Hz firing rate. The trains were separated by a small time difference Δt. We then determined the amplitude of the second transient relative to the first transient (Figure 3 A1). We found that inhibition was maximal at Δt = 200 ms - 400 ms and decayed over 2 s (Figure 3 A2, circles). The time course is similar to observations *in vivo* by Benoit-Marand et al (Benoit-Marand et al. 2001)(Figure 3 A2, asterisk) and in vitro by Phillips et al (Phillips et al. 2002). However, at $\Delta t < 100$ ms our model underestimates the trailing DA transient, probably because it does not include pulse-to-pulse facilitation.

Complex interplay between DA levels in the somatodendritic region, firing rate and terminal release

Our model couples somatic and terminal autoinhibition, two systems with different kinetics and behavior. When the DA system is perturbed from the resting state, for example by strong evoked release, the combined response of these systems may not be easily discerned experimentally. We therefore modeled typical experimental situations where transient release from DA neurons is evoked artificially.

We first investigated the case where tonic firing is interrupted by an evoked 0.5 s stimulus at 20 Hz firing rate (giving on average 10 spikes per DA neuron). The effective firing rate during the stimulus was assumed to overcome the effect of somatodendritic autoinhibition; only the spontaneous activity after the stimulus was affected.

The stimulus evoked a somatodendritic DA transient of 0.2 μM (Figure 3 B, solid) that in turn caused a temporal post stimulus depression in effective firing rate, from 4 Hz before the stimulus to 2.4 Hz after the stimulus. The slow decay of the somatodendritic DA transient lead to a relatively slow recovery of the effective firing rate (Figure 3 C, inset, solid).

In DS we observed DA transient of about 0.3 μM in amplitude (Figure 3 D, solid black). The onset of the transient was relatively fast. However, during the stimulus the release was reduced and the transient stagnated. This was mediated by temporal reduction of the release probability at the terminal level (Figure 3E, solid black). Thus saturation of terminal autoreceptors affected the shape of the transient.

We then calculated the effective firing rate following a strong stimulus, equivalent to 50 spikes at 60 Hz. Because the stimulus evoked a somatodendritic transient higher than 0.63 μM (Figure 3 B, dashed), we observed a complete stop in firing ($\nu_{eff} = 0$) lasting 3 s after termination of the stimulus and a depression of firing for up to 10 s after end of the stimulus (Figure 3 C, inset dashed). This may be compared to experimental observations by Kuhr et al., where electrical stimulation of the medial forebrain bundle by 120 pulses at 60 Hz caused a 90% reduction of DA cell firing in

394 the first 10 s and a 50% reduction of cell firing between 10 and 20 s after the
395 stimulus (Kuhr et al. 1987).

396 As a result of the high effective firing rate, we observed a 1.6 μM DA transient in DS.
397 The transient had biphasic shape, with quick onset transiting into a slower increase
398 phase 200-300 ms after onset of stimulus. After the stimulus the concentration of DA
399 reached 0 due to the post stimulus inhibition of firing rate (Figure 3 D and inset,
400 black dashed).

401 The strong stimulus evoked considerable increase in presynaptic autoinhibition.
402 During the 60 Hz stimulus, the release probability came close to the minimum value
403 of 2.5%. Interestingly, after the stimulus ended the long lasting depression of tonic
404 firing was compensated by a reduction in tonic terminal autoinhibition. Thus 3-8 s
405 after the stimulus terminal release probability was increased compared to the
406 resting value (Figure 3 E, black dashed).

407 Qualitative differences in autoreceptor control between DS and NAcc are often
408 observed experimentally (Zhang et al. 2009). It is not known whether these
409 differences are mediated directly by different autoreceptor architecture or in
410 directly, by differences in release and uptake. We therefore compared simulated
411 autoreceptor control of evoked release in NAcc and DS.

412 DAergic neurons that project to NAcc are located in ventral tegmental area (VTA)
413 whereas DAergic neurons in substantia nigra pars compacta (SNc) project to DS. For
414 simplicity we assumed that somatodendritic DA concentrations could be estimated
415 using same parameters. Therefore the evoked stimuli in either region shared

somatodendritic DA concentration and also the same effective firing rate (Figure 3 B and Figure 3 C). The transients produced by the same stimuli were of similar size but transients in NAcc appeared less bimodal and thus seemed less affected by terminal autoreceptors than in DS (Figure 3D, gray. Solid low stimulus, dashed high stimulus). However, the temporal evolution of the release probability in the two simulated regions was qualitatively similar (Figure 3E, gray). Thus, in our model, differences in release and uptake accounts for different shape of evoked transients in DS and NAcc.

Autoinhibition allows specific post synaptic integration of phasic DA signals

Bursts and pauses in firing of midbrain DA neurons are hypothesized to encode reward prediction errors giving crucial information for behavior (Bayer et al. 2007; Schultz 1998). Our model predicts that a brief burst will be followed by a long lasting somatodendritic depression in firing rate. Also, a pause in cell firing may evoke temporary increased firing rate after the pause. These effects oppose phasic signals and, if not carefully balanced, they could possibly quench their post synaptic integration. We therefore estimated how autoreceptors affected the post synaptic activation of high affinity (DRH) and low affinity (DRL) dopamine receptors to bursts and pauses.

We represented bursts by tonic activity interrupted by 21 Hz input firing rate (giving 20 Hz effective firing rate with the amount of autoinhibition generated by tonic somatodendritic DA levels). The bursts were of varying length between 0.05 s and 0.6 s, equivalent to 1-12 spikes at 20 Hz effective rate.

438 The effective firing rate during bursts was influenced by somatodendritic
439 autoinhibition. At burst onset, the effective firing rate was close to 20 Hz (Figure 4
440 A1). Hereafter, the effective firing rate decreased slightly during the burst and for
441 the longest burst the effective firing rate was 19 Hz at the end (Figure 4 B1). After
442 the burst, increased somatodendritic autoinhibition lead to lower effective tonic
443 firing rates: after the longest burst the tonic firing rate had dropped to 2.8 Hz (Figure
444 4 B1 inset).

445 The opposite effect was observed for pauses in firing patterns. Here there was a
446 transient decrease in somatodendritic DA levels (Figure 4 A2) and subsequent
447 increase up to 4.9 Hz in tonic firing rate (Figure 4 B2). In both cases the autoreceptor
448 compensation increased with the duration of the phasic signal.

449 Phasic DA levels in NAcc were affected by compensation of somatodendritic and
450 terminal autoreceptors. The bursts generated 0.2-0.4 μM DA transients in NAcc
451 (Figure 4 C1). The combination of somatodendritic and presynaptic autoinhibition
452 affected the shape of the transients especially from long bursts. Thus after the
453 transient DA levels in NAcc were reduced compared to tonic levels (Figure 4 C1) and
454 after pauses DA levels were temporarily increased (Figure 4 C2).

455 We then evaluated the effect of bursts and pauses on time resolved activity of high
456 and low affinity dopamine receptors. With tonic firing of DA neurons, the low affinity
457 DA receptors (DRL) were 6% activated. Bursts transiently increased activation to 20-
458 30% depending on burst length (Figure 4 D1). Tonic firing lead to 83% activation of
459 high affinity receptors (DRH). Here bursts transiently increased activation to 90-95%
460 depending on burst length (Figure 4 E1).

Autoreceptors dynamically affected activation of post synaptic receptors after the bursts. Under some circumstances these effects contributed with nearly equal magnitude as the phasic signal itself (Figure 4 E1, inset). We therefore quantified the impact of the burst on post synaptic DA receptors by calculating the change in area under curve (ΔAUC) of the receptor activation relative to the tonic baseline (Equation 10). Upward transient receptor activation above baseline gives a positive contribution to the AUC, downward transients gives a negative contribution. In our case a burst first gave a transient of high activation, contributing positively to the AUC (see for example Figure 4 E1, inset, dark gray area). Bursts were followed by a period of lower than average receptor activity which gave a negative contribution to the AUC (see for example Figure 4 E1, inset, dark gray area).

For low affinity receptors, the net change in AUC of the burst and subsequent autoreceptor inhibition was positive (Figure 4 F1, filled) even though autoreceptors reduced the postsynaptic signal (Figure 4 F1, asterisk).

On the other hand, the cancellation between positive and negative contributions to the ΔAUC strong for DRH receptors: Here the ΔAUC of the whole transient after the burst was nearly 0 (Figure 4 G1, filled), whereas the positive contribution was of similar magnitude as the influence of bursts on DRL (Figure 4 F1, circles). This indicates that autoreceptors strongly reduce the effect of isolated bursts when integrated by high affinity receptors.

For pauses there was a similar trend: Here the autoreceptor contribution was positive and competed with the negative AUC generated by the pause. Effectively

autoreceptors gave a 30% reduction in DRL signaling of pauses. On the other hand for DRH the compensation for pauses was hardly noticeable (Figure 4 F2 and G2).

Thus our model predicts that bursts affected the activation of low affinity receptors more than high affinity receptors (compare Figure 4 D1 and E1). Pauses in DA cell firing affected high affinity DA receptors more than low affinity receptors (compare Figure 4 D2 and E2). Autoreceptors increase the specificity in burst and pauses targeting low and high affinity receptor population.

Effect of DA uptake inhibition on dopamine signaling

The baseline level of extracellular DA in terminal and somatodendritic regions is sensitive to DA uptake inhibition. However, changes in uptake also evoke multiple compensatory responses of autoreceptors (Aragona et al. 2008; Einhorn et al. 1988; Rouge-Pont et al. 2002). The multiple competing effects make it difficult to deduce how DA uptake inhibitors affect DA signaling without the unified perspective on DA signaling offered by our model.

We first asked how different degrees of DA uptake inhibition would affect basal DA levels in NAcc.

In our model the coupling between somatodendritic dopamine levels and effective firing rate was deduced from experimental observations of firing rate as function of cocaine dose. Therefore, the modeled reductions in firing rate induced by uptake inhibition will by definition be in agreement with experimental data from Einhorn et al (Compare Figure 5 A1 with Figure 1 A) (Einhorn et al. 1988).

However, even though the firing rate was reduced, uptake inhibition increased the extracellular DA baseline in terminal regions of NAcc from 0.066 µM in the absence of uptake inhibition (K_{app} = 0.16 µM) to 0.134 µM with uptake inhibition equivalent to 15 mg/kg i.p. cocaine (K_{app} = 1.0 µM)(Figure 5 B1, compare blue and cyan, and Figure 5 E1, black circles).

DA uptake inhibition affected tonic activation of postsynaptic receptors. For DRL, the activation increased almost proportionally with increased DA levels (Figure 5 C1 and Figure 5 E1, red). On the other hand the change in activation of high affinity receptors was minor (Figure 5 D1 and Figure 5 E1, blue)

We then asked how DA uptake inhibition would affect post synaptic signaling when tonic firing was interrupted by a burst (Figure 5, second column).

The duration of the burst was 0.25 s, equivalent to 5 spikes at 20 Hz effective firing rate (Grace and Bunney 1984a). The firing rate during bursts was only slightly affected by DA uptake inhibition (Figure 5 A2). Bursts transiently increased the concentration of extracellular DA in NAcc. Without uptake inhibition the height of the transient was 0.23 µM (Figure 5 B2, blue). As uptake inhibition increased, the relative transient height remained nearly constant.

The transient changes in DA level were closely replicated by the activation of low affinity receptors (DRL, Figure 5 C2). In order to take into account the fact that uptake inhibition decreased the amplitude of transients but increased their width, we quantified the AUC of the transients compared to the baseline (Equation 10).

Then the net activation of low affinity receptors from bursts increased slightly (Figure 5 E2, red circles).

The integration of bursts by high affinity postsynaptic receptors (DRH) was only marginally affected by DA uptake inhibition: already 90% activated by tonic DA levels, the activity remained high in all conditions and was barely affected by DA uptake inhibition (Figure 5 D2 and Figure 5 E2, blue circles).

We then examined the effect of uptake inhibition on postsynaptic integration of a collective 1s pause in DA cell firing.

As DA uptake inhibition only affected the tonic firing rate, the effective firing rate during the pause was always 0 (Figure 5 A3 and inset).

In absence of uptake inhibition the extracellular DA in NAcc was evacuated within a few hundred milliseconds of the onset of the pause (Figure 5 B3, blue. See also Figure 4). The lowest DA level during the pause was less than 1 nM.

With low levels of uptake inhibition, the time course of the temporal depletion of DA during the pause was only slightly changed and the lowest DA level was 3 nM (Figure 5 B3, compare green and blue). With the highest level of DAT inhibition, the DA level remained above 50 nM in spite of the pause in cell firing (Figure 5 B3, cyan).

As before, activation of low affinity postsynaptic receptors was also sensitive to low DA level in terminal regions during the pause (Figure 5 C3). DAT inhibition had relatively little effect on the ΔAUC from the pause (Figure 5 E3, red). However, the ability of high affinity postsynaptic receptors to respond to pauses in DA neuron firing was dramatically reduced by DAT inhibition: the occurrence of low receptor

548 activation during the pause was strongly reduced even by low levels of uptake
549 inhibition (Figure 5 D3, compare blue and green) and it was completely extinguished
550 at intermediate levels and above (Figure 5 D3, compare blue with red or cyan, see
551 also Figure 5 E3, blue circles).

552 We then tested the effect of DA uptake inhibition on phasic signaling in DS. Here we
553 found similar change in basal DA level and in transient integration by low affinity
554 receptors as in NAcc (Figure 5 E1, dashed black, DS, and solid black, NAcc, are nearly
555 coincident. Figure 5 E2, compare dashed red, DS, and red circles, NAcc). However, in
556 comparison to NAcc, the integration of pauses by DS high affinity receptors was
557 substantially less affected by uptake inhibition. For values of K_{app} less than 0.35 μM
558 there was very little change in ΔAUC. For K_{app} above 0.35 μM, the response was
559 slower and full saturation was not observed (Figure 5 D3, inset, and Figure 5 E3,
560 dashed blue).

561 Interestingly, the value of K_{app} at which the DS high affinity receptor ΔAUC is reduced
562 by 50% corresponds to a dose of 15 mg/kg i.p. cocaine. This correlates with the
563 range of doses that lead to increased locomotor activity in rodents (Thomsen and
564 Caine 2011). In a recent study it was shown that mice with conditional knock out of
565 dopamine autoreceptors have increased sensitivity for the locomotor stimulating
566 effects of cocaine (Bello et al. 2011). We therefore asked if removal of autoreceptors
567 would also lead to increased sensitivity to uptake inhibition in our model. And in
568 particular we asked if saturation of high affinity receptors would occur at a lower
569 levels of uptake inhibition (removal of terminal autoreceptors was simulated by
570 setting P_{min} = 14% and removal of somatodendritic autoreceptors was simulated by

setting $\nu_{eff} = \nu_{in}$ regardless of somatodendritic DA levels. Other parameters were set for simulation of DS).

We found that DA levels increased much stronger with uptake inhibition in the absence of autoreceptors (Figure 5 E1, black asterisks). Also bursts gave terminal DA transients of the order of 1 μM. Initially the ΔAUC for low affinity receptors increased with uptake inhibition but was ultimately limited by saturation of the receptors (Figure 5 E2, red asterisks).

Importantly, high affinity receptors were less sensitive to pauses under uptake inhibition: A reduction of 50% of the AUC occurred with K_{app} = 0.55 μM, equivalent to 6.9 mg/kg ip cocaine in agreement with experiment (Bello et al. 2011) (Figure 5 E3, blue asterisks). Note: In absence of uptake inhibition the ΔAUC of the pause is slightly more negative in autoreceptor knock-out simulations than simulations of normal DS. This is because increased DA levels in autoreceptor knock out simulation giving higher tonic activation of the receptor before and after the pause.

Our estimates of P_{min} and P_{max} are subject to some experimental uncertainty, and biological variability in these variables is also expected. We therefore controlled for the sensitivity for details in our implementation by using a fixed amplitude model to predict post synaptic receptor activity (Dreyer et al. 2010). Here we found qualitatively similar results regarding the effect of DA inhibition on activation of post synaptic receptors.

Discussion

The model we present here involves a number of simplifications. For example, we did not include facilitation of DA release during burst firing (Montague et al. 2004). The effect of this assumption is apparent in our pair pulse study on short time scales where predictions of our model are lower compared to the *in vivo* observations (Figure 3 A2, compare blue and green at $\Delta t < 0.1$ s) (Benoit-Marand et al. 2001). Also, since the aim of this study was to describe fast time-scale modulation by autoreceptors we did not take limited dopamine stores into account and autoreceptor regulation of the DA synthesis (Beaulieu and Gainetdinov 2011).

We described autoreceptors from a systems level perspective. In this spirit we connected the occupancy of presynaptic autoreceptors directly to the terminal release probability and firing rate, omitting calculation of ionic currents mediated by GIRK channels associated with autoreceptors. The finite on and off rate of DA with autoreceptors was included for terminal autoreceptors only. This assumption implicitly assumes that the interaction between DA and somatodendritic autoreceptors is much faster than variations in somatodendritic DA concentration (Beckstead et al. 2004; John et al. 2006).

In our study, DA uptake inhibition increased the basal DA level monotonically but not linearly (Figure 5 E1, black circles). In comparison a meta analysis of microdialysis studies by Frank et al. (Frank et al. 2008) revealed a linear correlation between relative increase in basal DA level and ip administered dose of cocaine in mg/kg (Frank et al. 2008). At low or moderate doses our model agrees relatively well with the analysis by Frank et al.: For $K_{app} < 0.5$ μM (equivalent to ip cocaine less than 6

614 mg/kg) our model predicts increase tonic DA levels which agree by more than 80% of
615 the result by Frank. However at uptake inhibition equivalent 20 mg/kg cocaine our
616 model predicts only half the increase observed by Frank et al. In this respect it is also
617 worth noting that we determined the somatodendritic influence on firing rates from
618 empirical data of animals under anesthesia (Einhorn et al. 1988) where cocaine
619 reduces the firing rate to greater extent than recently observed in freely moving
620 animals (Koulchitsky et al. 2012). We believe this could lead to our model
621 underestimating the increase in DA by high doses of cocaine.

622 Our model of somatodendritic DA levels (Equation 4) is based on voltammetry data
623 from mouse slices (John et al. 2006). We found somatodendritic DA transients on the
624 order of 100 nM, which is in relatively good agreement with other voltammetry
625 observations in anesthetized rats (Kita et al. 2009) and in guinea pig slices (Rice et al.
626 1997). On the other hand, our calculated tonic somatodendritic DA levels are higher
627 than the 1 nM level reported with microdialysis (Kalivas and Duffy 1993). However,
628 calculation of absolute DA levels from microdialysis measurements is a complex
629 problem. Elaborate models suggest that tissue damage near dialysis probes influence
630 measurements of basal DA levels (Borland et al. 2005; Bungay et al. 2003). Our
631 model, on the other hand, is based on a minimal number of experimentally
632 determined assumptions, and does not take such effects into account. We therefore
633 choose to test our model by predicting dynamical aspects of DA signaling where
634 experimental data is less subject to such artifacts (Peters et al. 2004).

635 To our knowledge, the present model constitutes the first integrated description of
636 DA signaling and how this is affected by both terminal and somatodendritic DA

637 autoreceptors and DA uptake inhibition. Our analyses revealed a multitude of
638 experimentally relevant dynamical effects of the dual autoreceptor system. We
639 predict that somatodendritic autoinhibition exerts indirect influence on terminal
640 release: Strong evoked release induced a reduction of tonic cell firing which lead to
641 facilitation of terminal release 3-8 s after the transient (Figure 3E). Even though the
642 compensatory effects of autoreceptors are appreciable, they do not invalidate our
643 previous estimates of the post synaptic response to phasic reward related signals
644 (Dreyer et al. 2010): Low affinity receptors were sensitive to bursts and high affinity
645 receptors were mostly sensitive to pauses (Figure 4 F1 and G2). Autoreceptors
646 strongly compensated the effect of bursts on high affinity receptors and also
647 reduced the effect of pauses on low affinity receptors which increases selectivity of
648 bursts and pauses in targeting different receptor populations (Figure 4 G1 and Figure
649 4F1).

650 We applied the model to the case of DA uptake inhibition and investigated how this
651 would affect post synaptic integration of tonic and phasic DA signals. Our model was
652 in agreement with experimental studies suggesting a strong influence of DA
653 autoreceptors in the effect of cocaine (Aragona et al. 2008; Bello et al. 2011; Rouge-
654 Pont et al. 2002).

655 The most prominent post synaptic effect of uptake inhibition was that high affinity
656 receptors (DRH) decoupled from pauses in phasic firing patters (Figure 5 C). At
657 certain levels of uptake inhibition DRH receptor signaling underwent a transition
658 from phasic (DRH activation sensitive to pauses in firing pattern) to essentially tonic
659 (DRH tonically activated regardless of firing pattern). In NAcc high affinity receptor

660 decoupling occurred at therapeutic levels of uptake inhibition, similar to 2.7 mg/kg
661 i.p. methylphenidate (MP). In DS same degree of decoupling occurred with uptake
662 inhibition close to locomotor stimulating doses around 15 mg/kg i.p. cocaine
663 (Thomsen and Caine 2011). Removal of autoreceptor control lead to decoupling at
664 lower levels of uptake inhibition, similar to 7 mg/kg i.p cocaine.

665 Obviously the exact location of the transition from phasic to tonic activation of DRH
666 is depending on our choice of 1 s as a 'typical' length of a pause in DAergic firing. We
667 also tested high and low affinity receptor activation with a phasic firing pattern
668 containing a distribution of bursts and pauses of different length. Here short pauses
669 were decoupled at even lower levels of uptake inhibition while post synaptic
670 integration of long pauses was reliable at higher levels of uptake inhibition and with
671 similar differences between NAcc and DS (not shown). Pauses in DA cell firing
672 observed in classical reward prediction experiments are on the order of 200-400 ms
673 (Bayer et al. 2007; Schultz 1998). However in other experimental paradigms the
674 inhibition of DA neuronal activity may last several seconds (Mileykovskiy and
675 Morales 2011) and 1 second pauses in firing are relatively common in phasic firing
676 patterns, see examples in Bingmer et al (Bingmer et al. 2011)).

677 Dopamine D1-like and D2-like receptors have both high affinity and low affinity
678 states for agonist binding (May 1992). However indisputable determination of the
679 biological function of these states is still lacking (Skinbjerg et al. 2012). Our
680 implementation of autoreceptors embraces this range of affinities: The high
681 somatodendritic DA levels required to reduce effective firing rate implicitly assumes

682 low affinity of somatodendritic D2 autoreceptors whereas our presynaptic D2
683 autoreceptors are assumed to have EC50 ≈ 40 nM.

684 Assuming that postsynaptic D2 receptors are predominantly in the high affinity state
685 and that D1 receptors are in low affinity state, our model complies *in vivo* studies
686 showing high tonic activity of D2 receptors (Bertran-Gonzalez et al. 2008;
687 Svenningsson et al. 2000). However, this raises new questions because D2 receptors
688 are often ascribed an important role in mediating hyperlocomotor effects of DA
689 uptake inhibitors (Chausmer and Katz 2001). How can this be possible if they are
690 already saturated by spontaneous DAergic activity? We resolve this problem by
691 considering high affinity D2 receptors to be modulated by a dynamic DA signal. In
692 the unperturbed state, pauses in DA cell firing constitute an efficient method for
693 mediating time resolved signals to high affinity receptors. However, this signal is
694 crucially dependent on DATs to remove extracellular DA during the pause. Therefore
695 low and intermediate doses of DA uptake strongly modulate or even block this part
696 of the DA signal with sensitivity inversely dependent on V_{max}.

697 Under the hypothesis that DRH describes the majority of D2 receptors and DRL
698 describes D1 receptors, our model predicts that DA uptake inhibitors will influence
699 post synaptic targets differently depending on activity state of DA neurons. With
700 *tonically* firing DA neurons DAT inhibitors mainly increase D1 receptor activation but
701 leave D2 activation largely unaffected (Figure 5 E1). This is similar to observations by
702 Svenningson et al (Svenningsson et al. 2000) and by Bertran-Gonzales et al (Bertran-
703 Gonzalez et al. 2008). However, with *phasically* firing DA neurons, where firing
704 patterns include bursts and pauses, both D1 and D2 signaling is affected. As a

corollary, our model predicts that in experimental paradigms associated with increased phasic signaling, such as stress (Anstrom et al. 2009; Valenti et al. 2011), locomotor responses to DA uptake inhibition will be augmented compared to experimental situations where DA signal is dominated by tonic firing.

The exact role of DA in the therapeutic mechanism of psychostimulant medication of ADHD is debated (Gonon 2009; Volkow et al. 2010). Even though the present results suggest that significant changes in high affinity receptor signaling can occur at therapeutic doses, this does not exclude that other mechanisms, such as nor-adrenalin or DA signaling in prefrontal cortex, mediates the therapeutically beneficial action of methylphenidate in ADHD (Berridge et al. 2006). Thus it may as well be that the changes in phasic DA signaling we observe is an adverse effect and that the therapeutically optimal dose has minimal influence.

In summary, our mathematical model provides the unified description of the link between somatodendritic DA release, firing patterns of DA neurons and pre- and post synaptic DA receptor activation. We used this model to show that the qualitative effect of DAT inhibition depends strongly on the firing patterns of DA neurons and indentified critical levels of uptake inhibition at which high affinity DA receptor signaling looses sensitivity to pauses in DA cell firing. In NAcc this effect occurred in the therapeutic range of DAT inhibition whereas high affinity receptors in DS were sensitive to higher levels that induce locomotor symptoms in behaving animals.

Grants

Jakob Kisbye Dreyer is supported by the Lundbeck Foundation (grant number R77-A6926).

Disclosures

No conflicts of interest, financial or otherwise, are declared by the authors.

Figure captions

Figure 1

Construction of somatodendritic autoreceptor feedback. Panel A: Firing rates from Einhorn et al (Einhorn et al. 1988) plotted against estimated apparent uptake constant using Equation 3. Firing rate was put on an absolute scale assuming 4 Hz firing rate in the control case. Filled markers indicate the 3 conditions plotted in Panel B. Panel B: Concentration of somatodendritic DA using the combination of firing rate and estimated apparent uptake constant shown in Panel A. The 3 conditions correspond to ν_{eff} = 4 Hz and K_{app} = *0.16 μM* (lowest line), ν_{eff} = 3.4 Hz and K_{app} = *0.40 μM* (middle line), and ν_{eff} = 2.1 Hz and K_{app} = *1.35 μM* (top line). Panel C: Einhorn firing rate plotted against numerically determined somatodendritic DA levels, filled markers indicate the conditions shown in B. Dashed line: Effective firing rate as given by Equation 5.

Figure 2

Construction of terminal DA release and presynaptic autoreceptor feedback. Panel A: spatial distribution of DA in terminal simulation space during tonic firing. Color indicates extracellular concentration of DA as indicated on the color bar. Black dots

indicate DA release sites. Note that the volume is filled with 1500 DA release sites and only those close to the boundary are visible on this plot. In order to better illustrate 3D heterogeneity of DA concentration, the image has higher spatial resolution than during typical simulations. Panel B: Distribution of DA uptake capacity in a section through the simulation space in the *yz*-plane. Color indicates V_{max}. The spatial resolution is as in typical simulations. Panel C: Relation between equilibrium DA levels and release probability, P_r. Dashed black line shows the resting value of P_r and baseline DA levels under 4 Hz tonic firing. Panel D: Release probability of different terminals. Black line indicates average.

Figure 3

Analysis of interaction between somatodendritic and terminal autoinhibition with evoked release. Panel A1: Data from pair pulse simulation. Each transient was evoked by simulating a train of 3 pulses at 100 Hz, each train was separated by Δt. Height of first transient is denoted P_1 and the height of the second transient P_2. Panel A2: Circles, P_2/P_1 as function of Δt; asterisks, experimental data reproduced from Benoit-Marand et al (Benoit-Marand et al. 2001). In Panels B, C, D, and E dashed lines indicate strong stimulus (50 spikes at 60 Hz), and solid lines indicate light stimulus (10 spikes at 20 Hz). Panel B: Somatodendritic DA levels from stimulated release and tonic firing rate. The plot shows 2 cycles each of 10 s. Panel C: Effective firing rate of DA neurons corresponding to somatic DA levels in Panel B. Inset in C: Close view of effective firing rate during one stimulus cycle. Note that during stimulated release, the effective firing rate is not affected by autoinhibition.

776 Panel D: Resulting DA levels in terminal regions. Results for DS are shown in black
777 and NAcc in gray. Inset in D: Close view of DS DA levels after strong stimulus. Panel E:
778 Concurrent release probability at the terminal level, same colors as in Panel D.

779

780

781

782

783 Figure 4

784 Autoreceptor influence on DA phasic signals. Panel A1: somatodendritic DA levels
785 during bursts (Δt_{burst}= 0.1 s, 0.3 s, and 0.6 s). Panel B1: Concurrent effective firing
786 rate. Inset in B1: Close view of firing rates. Panel C1: DA levels in NAcc. Panel D1:
787 Activation of low affinity receptors (DRL) during bursts. Panel E1: Activation of high
788 affinity receptors (DRH) during bursts. Inset in E1: schematic illustration of positive
789 (dark gray) and negative (light gray) contributions to the ΔAUC. Panel F1: ΔAUC of
790 DRL activity from bursts of duration Δt_{burst}. Circles: total ΔAUC including positive and
791 negative contributions. Asterisk: positive part of the peak only. Panel G1: ΔAUC of
792 DRH from bursts, same markers as in Panel F1. Panel A2: Somatodendritic DA levels
793 during pauses (Δt_{pause} = 0.8 s, 1.6 s, 2.4 s). Panel B2: Effective firing rate during and
794 after the pauses. Panel C2: DA levels in NAcc. Panel D2: Activation of DRL during
795 pauses. Panel E1: Activation of DRH during pauses. Panel F2: ΔAUC of DRL activity
796 during pauses. Circles: Negative contribution only. Asterisk: Total AUC including

positive compensation by autoreceptors. Panel G2: ΔAUC of DRH for pauses, same markers as in Panel F2.

Figure 5

Influence of DA uptake inhibition on the post synaptic effect of phasic DA signaling. Except where noted the figure shows results for simulations of NAcc. Colors in A-D indicate different values of K_{app}. Blue, K_{app}=0.16 μM (control); green, K_{app} = 0.35 μM; red K_{app} = 0.7 μM; and cyan, K_{app} = 1 μM. Panels A1-E1 show the effect of uptake inhibition on tonic firing. Panels A2-E2 show a burst (Δt_{burst} = 0.25 s). Panels A3-E3 show the effect of a pause (Δt_{pause} = 1 s). Panels A1- A3 show effective firing rate as function of time. Insets in A2 and A3 show close view of firing rate around the burst/pause. Panels B1-B3 show space averaged DA levels, panels C1-C3 show DRL activation, and panels D1-D3 show DRH activation. Inset in Panel D3: Activation of DS DRH during pauses. Color code for panels E1-E3: Black, DA levels; red, DRL; and blue, DRH. Line styles in Panels E1-E3: Solid lines with circles, NAcc signals. Dashed lines: DS signals. Dashed with asterisks: autoreceptor knock-out simulations. Panel E1 shows relative increase in tonic signaling as function of K_{app}. Panel E2 shows change in ΔAUC from bursts. Panel E3: ΔAUC from pause.

References

Anstrom KK, Miczek KA, and Budygin EA. Increased phasic dopamine signaling in the mesolimbic pathway during social defeat in rats. *Neuroscience* 161: 3-12, 2009.
Aragona BJ, Cleaveland NA, Stuber GD, Day JJ, Carelli RM, and Wightman RM. Preferential enhancement of dopamine transmission within the nucleus accumbens shell by cocaine is attributable to a direct increase in phasic dopamine release events. *J Neurosci* 28: 8821-8831, 2008.
Bayer HM, Lau B, and Glimcher PW. Statistics of midbrain dopamine neuron spike trains in the awake primate. *Journal of Neurophysiology* 98: 1428-1439, 2007.
Beaulieu JM, and Gainetdinov RR. The physiology, signaling, and pharmacology of dopamine receptors. *Pharmacol Rev* 63: 182-217, 2011.
Beckstead MJ, Grandy DK, Wickman K, and Williams JT. Vesicular dopamine release elicits an inhibitory postsynaptic current in midbrain dopamine neurons. *Neuron* 42: 939-946, 2004.
Bello EP, Mateo Y, Gelman DM, Noain D, Shin JH, Low MJ, Alvarez VA, Lovinger DM, and Rubinstein M. Cocaine supersensitivity and enhanced motivation for reward in mice lacking dopamine D2 autoreceptors. *Nat Neurosci* 14: 1033-1038, 2011.
Benoit-Marand M, Borrelli E, and Gonon F. Inhibition of dopamine release via presynaptic D2 receptors: time course and functional characteristics in vivo. *J Neurosci* 21: 9134-9141, 2001.
Berridge CW, Devilbiss DM, Andrzejewski ME, Arnsten AFT, Kelley AE, Schmeichel B, Hamilton C, and Spencer RC. Methylphenidate preferentially increases catecholamine neurotransmission within the prefrontal cortex at low doses that enhance cognitive function. *Biol Psychiat* 60: 1111-1120, 2006.
Bertran-Gonzalez J, Bosch C, Maroteaux M, Matamales M, Herve D, Valjent E, and Girault JA. Opposing patterns of signaling activation in dopamine D1 and D2 receptor-expressing striatal neurons in response to cocaine and haloperidol. *J Neurosci* 28: 5671-5685, 2008.
Bingmer M, Schiemann J, Roeper J, and Schneider G. Measuring burstiness and regularity in oscillatory spike trains. *J Neurosci Methods* 201: 426-437, 2011.
Borland LM, Shi G, Yang H, and Michael AC. Voltammetric study of extracellular dopamine near microdialysis probes acutely implanted in the striatum of the anesthetized rat. *J Neurosci Methods* 146: 149-158, 2005.
Buckholtz JW, Treadway MT, Cowan RL, Woodward ND, Li R, Ansari MS, Baldwin RM, Schwartzman AN, Shelby ES, Smith CE, Kessler RM, and Zald DH. Dopaminergic network differences in human impulsivity. *Science* 329: 532, 2010.
Bungay PM, Newton-Vinson P, Isele W, Garris PA, and Justice JB. Microdialysis of dopamine interpreted with quantitative model incorporating probe implantation trauma. *J Neurochem* 86: 932-946, 2003.
Chance B. The kinetics of the enzyme-substrate compound of peroxidase. *Journal of Biological Chemistry* 151: 553-577, 1943.

Chausmer AL, and Katz JL. The role of D2-like dopamine receptors in the locomotor stimulant effects of cocaine in mice. *Psychopharmacology (Berl)* 155: 69-77, 2001.
Cools R, and D'Esposito M. Inverted-U-shaped dopamine actions on human working memory and cognitive control. *Biol Psychiatry* 69: e113-125, 2011.
Cragg SJ, and Greenfield SA. Differential autoreceptor control of somatodendritic and axon terminal dopamine release in substantia nigra, ventral tegmental area, and striatum. *J Neurosci* 17: 5738-5746, 1997.
Cragg SJ, and Rice ME. DAncing past the DAT at a DA synapse. *Trends Neurosci* 27: 270-277, 2004.
Dagher A, and Robbins TW. Personality, Addiction, Dopamine: Insights from Parkinson's Disease. *Neuron* 61: 502-510, 2009.
Doucet G, Descarries L, and Garcia S. Quantification of the dopamine innervation in adult rat neostriatum. *Neuroscience* 19: 427-445, 1986.
Dreyer JK, Herrik KF, Berg RW, and Hounsgaard JD. Influence of phasic and tonic dopamine release on receptor activation. *J Neurosci* 30: 14273-14283, 2010.
Dugast C, Brun P, Sotty F, Renaud B, and SuaudChagny MF. On the involvement of a tonic dopamine D2-autoinhibition in the regulation of pulse-to-pulse-evoked dopamine release in the rat striatum in vivo. *N-S Arch Pharmacol* 355: 716-719, 1997.
Einhorn LC, Johansen PA, and White FJ. Electrophysiological effects of cocaine in the mesoaccumbens dopamine system: studies in the ventral tegmental area. *J Neurosci* 8: 100-112, 1988.
el Mestikawy S, Glowinski J, and Hamon M. Presynaptic dopamine autoreceptors control tyrosine hydroxylase activation in depolarized striatal dopaminergic terminals. *J Neurochem* 46: 12-22, 1986.
Espana RA, Roberts DC, and Jones SR. Short-acting cocaine and long-acting GBR-12909 both elicit rapid dopamine uptake inhibition following intravenous delivery. *Neuroscience* 155: 250-257, 2008.
Frank ST, Krumm B, and Spanagel R. Cocaine-induced dopamine overflow within the nucleus accumbens measured by in vivo microdialysis: A meta-analysis. *Synapse* 62: 243-252, 2008.
Garris PA, Ciolkowski EL, Pastore P, and Wightman RM. Efflux of dopamine from the synaptic cleft in the nucleus accumbens of the rat brain. *J Neurosci* 14: 6084-6093, 1994a.
Garris PA, Ciolkowski EL, and Wightman RM. Heterogeneity of evoked dopamine overflow within the striatal and striatoamygdaloid regions. *Neuroscience* 59: 417-427, 1994b.
Gonon F. The dopaminergic hypothesis of attention-deficit/hyperactivity disorder needs re-examining. *Trends Neurosci* 32: 2-8, 2009.
Gonon FG, and Buda MJ. Regulation of dopamine release by impulse flow and by autoreceptors as studied by in vivo voltammetry in the rat striatum. *Neuroscience* 14: 765-774, 1985.
Grace AA, and Bunney BS. The control of firing pattern in nigral dopamine neurons: burst firing. *J Neurosci* 4: 2877-2890, 1984a.
Grace AA, and Bunney BS. The control of firing pattern in nigral dopamine neurons: single spike firing. *J Neurosci* 4: 2866-2876, 1984b.

Grace AA, Floresco SB, Goto Y, and Lodge DJ. Regulation of firing of dopaminergic neurons and control of goal-directed behaviors. *Trends Neurosci* 30: 220-227, 2007.
Herr NR, Daniel KB, Belle AM, Carelli RM, and Wightman RM. Probing presynaptic regulation of extracellular dopamine with iontophoresis. *ACS Chem Neurosci* 1: 627-638, 2010.
Hersch SM, Yi H, Heilman CJ, Edwards RH, and Levey AI. Subcellular localization and molecular topology of the dopamine transporter in the striatum and substantia nigra. *J Comp Neurol* 388: 211-227, 1997.
Howes OD, and Kapur S. The dopamine hypothesis of schizophrenia: version III--the final common pathway. *Schizophr Bull* 35: 549-562, 2009.
Hyland BI, Reynolds JN, Hay J, Perk CG, and Miller R. Firing modes of midbrain dopamine cells in the freely moving rat. *Neuroscience* 114: 475-492, 2002.
John CE, Budygin EA, Mateo Y, and Jones SR. Neurochemical characterization of the release and uptake of dopamine in ventral tegmental area and serotonin in substantia nigra of the mouse. *J Neurochem* 96: 267-282, 2006.
John CE, and Jones SR. Voltammetric characterization of the effect of monoamine uptake inhibitors and releasers on dopamine and serotonin uptake in mouse caudate-putamen and substantia nigra slices. *Neuropharmacology* 52: 1596-1605, 2007.
Kalivas PW, and Duffy P. Time course of extracellular dopamine and behavioral sensitization to cocaine. II. Dopamine perikarya. *J Neurosci* 13: 276-284, 1993.
Kita JM, Kile BM, Parker LE, and Wightman RM. In vivo measurement of somatodendritic release of dopamine in the ventral tegmental area. *Synapse* 63: 951-960, 2009.
Koulchitsky S, De Backer B, Quertemont E, Charlier C, and Seutin V. Differential effects of cocaine on dopamine neuron firing in awake and anesthetized rats. *Neuropsychopharmacology* 37: 1559-1571, 2012.
Kuhr WG, Wightman RM, and Rebec GV. Dopaminergic-Neurons - Simultaneous Measurements of Dopamine Release and Single-Unit Activity during Stimulation of the Medial Forebrain-Bundle. *Brain Research* 418: 122-128, 1987.
May T. Striatal Dopamine-D1-Like Receptors Have Higher Affinity for Dopamine in Ethanol-Treated Rats. *European Journal of Pharmacology* 215: 313-316, 1992.
Mileykovskiy B, and Morales M. Duration of inhibition of ventral tegmental area dopamine neurons encodes a level of conditioned fear. *J Neurosci* 31: 7471-7476, 2011.
Moller HJ. Antipsychotic and antidepressive effects of second generation antipsychotics: two different pharmacological mechanisms? *Eur Arch Psychiatry Clin Neurosci* 255: 190-201, 2005.
Montague PR, McClure SM, Baldwin PR, Phillips PEM, Budygin EA, Stuber GD, Kilpatrick MR, and Wightman RM. Dynamic gain control of dopamine delivery in freely moving animals. *J Neurosci* 24: 1754-1759, 2004.
Moquin KF, and Michael AC. Tonic autoinhibition contributes to the heterogeneity of evoked dopamine release in the rat striatum. *J Neurochem* 110: 1491-1501, 2009.

Oleson EB, Salek J, Bonin KD, Jones SR, and Budygin EA. Real-time voltammetric detection of cocaine-induced dopamine changes in the striatum of freely moving mice. *Neurosci Lett* 467: 144-146, 2009.
Peters JL, Miner LH, Michael AC, and Sesack SR. Ultrastructure at carbon fiber microelectrode implantation sites after acute voltammetric measurements in the striatum of anesthetized rats. *J Neurosci Methods* 137: 9-23, 2004.
Phillips PE, Hancock PJ, and Stamford JA. Time window of autoreceptor-mediated inhibition of limbic and striatal dopamine release. *Synapse* 44: 15-22, 2002.
Pickel VM, Johnson E, Carson M, and Chan J. Ultrastructure of spared dopamine terminals in caudate-putamen nuclei of adult rats neonatally treated with intranigral 6-hydroxydopamine. *Brain Res Dev Brain Res* 70: 75-86, 1992.
Pucak ML, and Grace AA. Evidence That Systemically Administered Dopamine Antagonists Activate Dopamine Neuron Firing Primarily by Blockade of Somatodendritic Autoreceptors. *Journal of Pharmacology and Experimental Therapeutics* 271: 1181-1192, 1994.
Rice ME, Cragg SJ, and Greenfield SA. Characteristics of electrically evoked somatodendritic dopamine release in substantia nigra and ventral tegmental area in vitro. *J Neurophysiol* 77: 853-862, 1997.
Rouge-Pont F, Usiello A, Benoit-Marand M, Gonon F, Piazza PV, and Borrelli E. Changes in extracellular dopamine induced by morphine and cocaine: crucial control by D2 receptors. *J Neurosci* 22: 3293-3301, 2002.
Schmitz Y, Benoit-Marand M, Gonon F, and Sulzer D. Presynaptic regulation of dopaminergic neurotransmission. *J Neurochem* 87: 273-289, 2003.
Schultz W. Predictive reward signal of dopamine neurons. *J Neurophysiol* 80: 1-27, 1998.
Skinbjerg M, Sibley DR, Javitch JA, and Abi-Dargham A. Imaging the high-affinity state of the dopamine D2 receptor in vivo: fact or fiction? *Biochem Pharmacol* 83: 193-198, 2012.
Svenningsson P, Lindskog M, Ledent C, Parmentier M, Greengard P, Fredholm BB, and Fisone G. Regulation of the phosphorylation of the dopamine- and cAMP-regulated phosphoprotein of 32 kDa in vivo by dopamine D1, dopamine D2, and adenosine A2A receptors. *Proc Natl Acad Sci U S A* 97: 1856-1860, 2000.
Thomsen M, and Caine SB. Psychomotor stimulant effects of cocaine in rats and 15 mouse strains. *Exp Clin Psychopharmacol* 19: 321-341, 2011.
Valenti O, Lodge DJ, and Grace AA. Aversive Stimuli Alter Ventral Tegmental Area Dopamine Neuron Activity via a Common Action in the Ventral Hippocampus. *J Neurosci* 31: 4280-4289, 2011.
Venton BJ, Zhang H, Garris PA, Phillips PE, Sulzer D, and Wightman RM. Real-time decoding of dopamine concentration changes in the caudate-putamen during tonic and phasic firing. *J Neurochem* 87: 1284-1295, 2003.
Volkow ND, Wang GJ, Fowler JS, Gatley SJ, Logan J, Ding YS, Hitzemann R, and Pappas N. Dopamine transporter occupancies in the human brain induced by therapeutic doses of oral methylphenidate. *Am J Psychiatry* 155: 1325-1331, 1998.
Volkow ND, Wang GJ, Newcorn JH, Kollins SH, Wigal TL, Telang F, Fowler JS, Goldstein RZ, Klein N, Logan J, Wong C, and Swanson JM. Motivation deficit in

ADHD is associated with dysfunction of the dopamine reward pathway. *Mol Psychiatry* 2010.
Wallace LJ, and Hughes RM. Computational analysis of stimulated dopaminergic synapses suggests release largely occurs from a single pool of vesicles. *Synapse* 62: 909-919, 2008.
Wightman RM, Heien MLAV, Wassum KM, Sombers LA, Aragona BJ, Khan AS, Ariansen JL, Cheer JF, Phillips PEM, and Carelli RM. Dopamine release is heterogeneous within microenvironments of the rat nucleus accumbens. *Eur J Neurosci* 26: 2046-2054, 2007.
Wightman RM, and Zimmerman JB. Control of dopamine extracellular concentration in rat striatum by impulse flow and uptake. *Brain Res Brain Res Rev* 15: 135-144, 1990.
Wu Q, Reith ME, Walker QD, Kuhn CM, Carroll FI, and Garris PA. Concurrent autoreceptor-mediated control of dopamine release and uptake during neurotransmission: an in vivo voltammetric study. *J Neurosci* 22: 6272-6281, 2002.
Zhang L, Doyon WM, Clark JJ, Phillips PE, and Dani JA. Controls of tonic and phasic dopamine transmission in the dorsal and ventral striatum. *Mol Pharmacol* 76: 396-404, 2009.

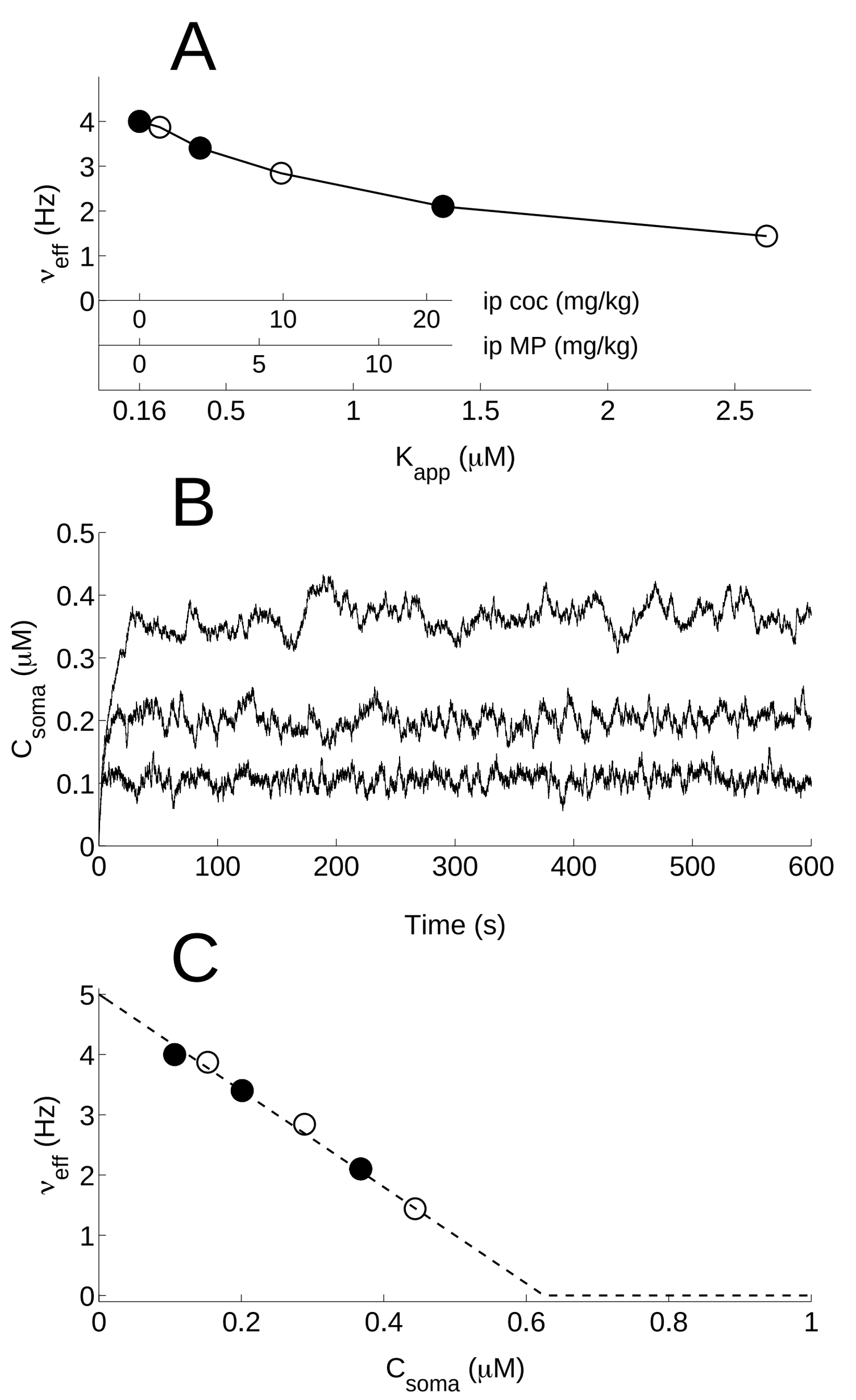
A
ν_{eff} (Hz)
0
1
2
3
4
ip coc (mg/kg)
0
10
20
ip MP (mg/kg)
0
5
10
0.16
0.5
1
1.5
2
2.5
K_{app} (μM)
B
C_{soma} (μM)
0
0.1
0.2
0.3
0.4
0.5
0
100
200
300
400
500
600
Time (s)
C
ν_{eff} (Hz)
0
1
2
3
4
5
0
0.2
0.4
0.6
0.8
1
C_{soma} (μM)

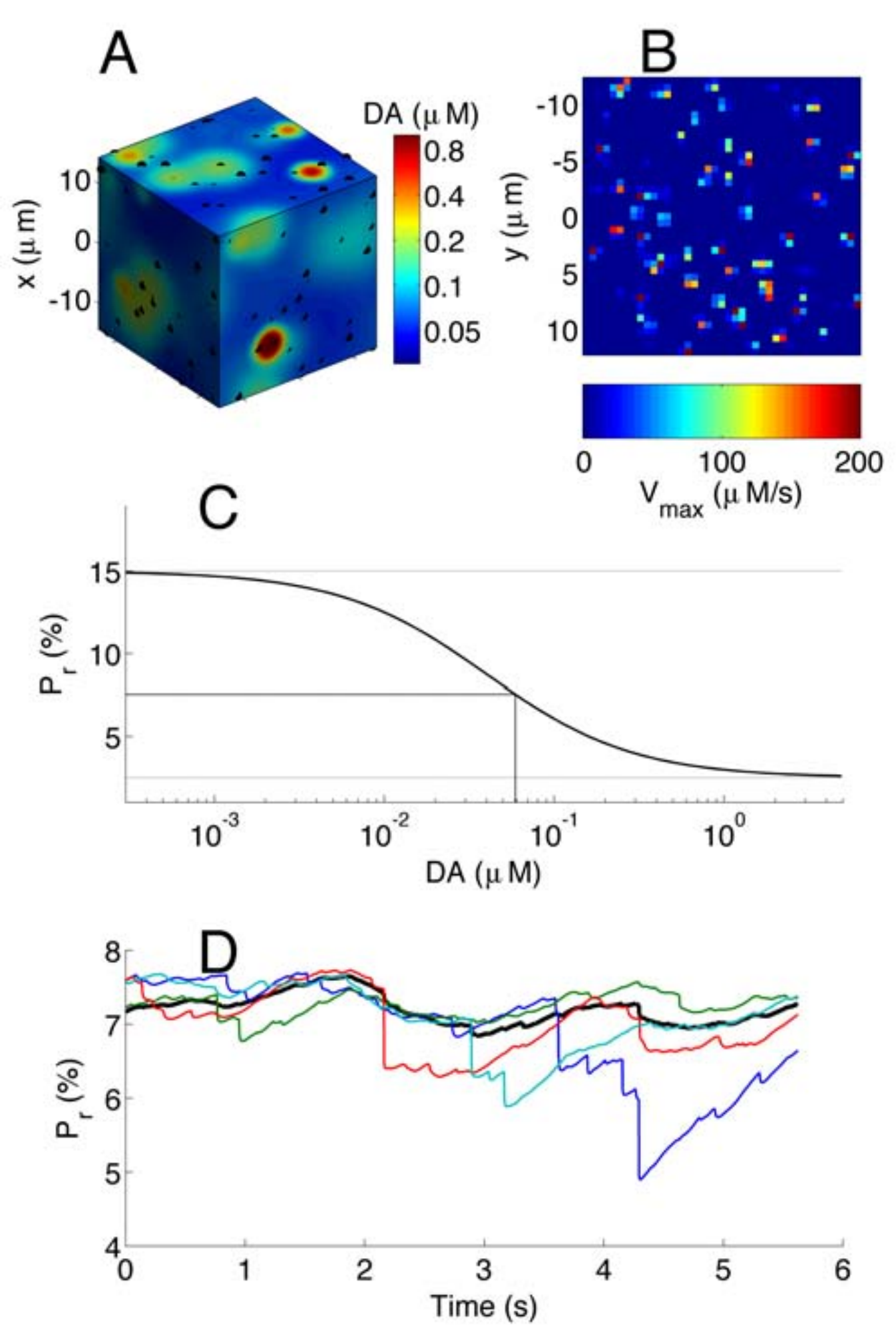
A
DA (μ M)
0.8
0.4
0.2
0.1
0.05
x (μ m)
10
0
-10
B
y (μ m)
-10
-5
0
5
10
0
100
200
V max (μ M/s)
C
P r (%)
15
10
5
10 -3
10 -2
10 -1
10 0
DA (μ M)
D
P r (%)
8
7
6
5
4
0
1
2
3
4
5
6
Time (s)

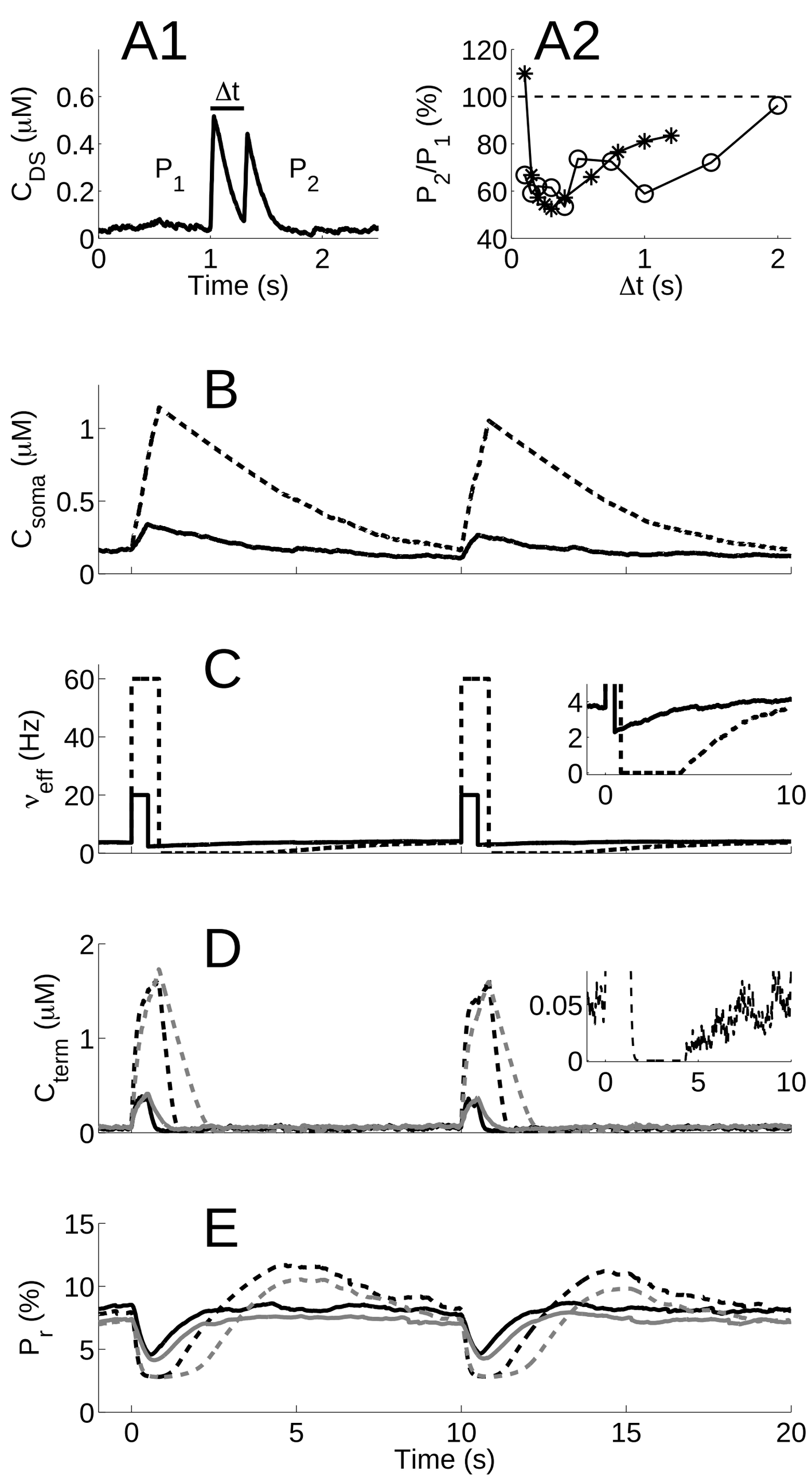
A1
A2
B
C
D
E
C_{DS} (μM)
Δt
P_1
P_2
Time (s)
P_2/P_1 (%)
Δt (s)
C_{soma} (μM)
ν_{eff} (Hz)
C_{term} (μM)
P_r (%)
Time (s)

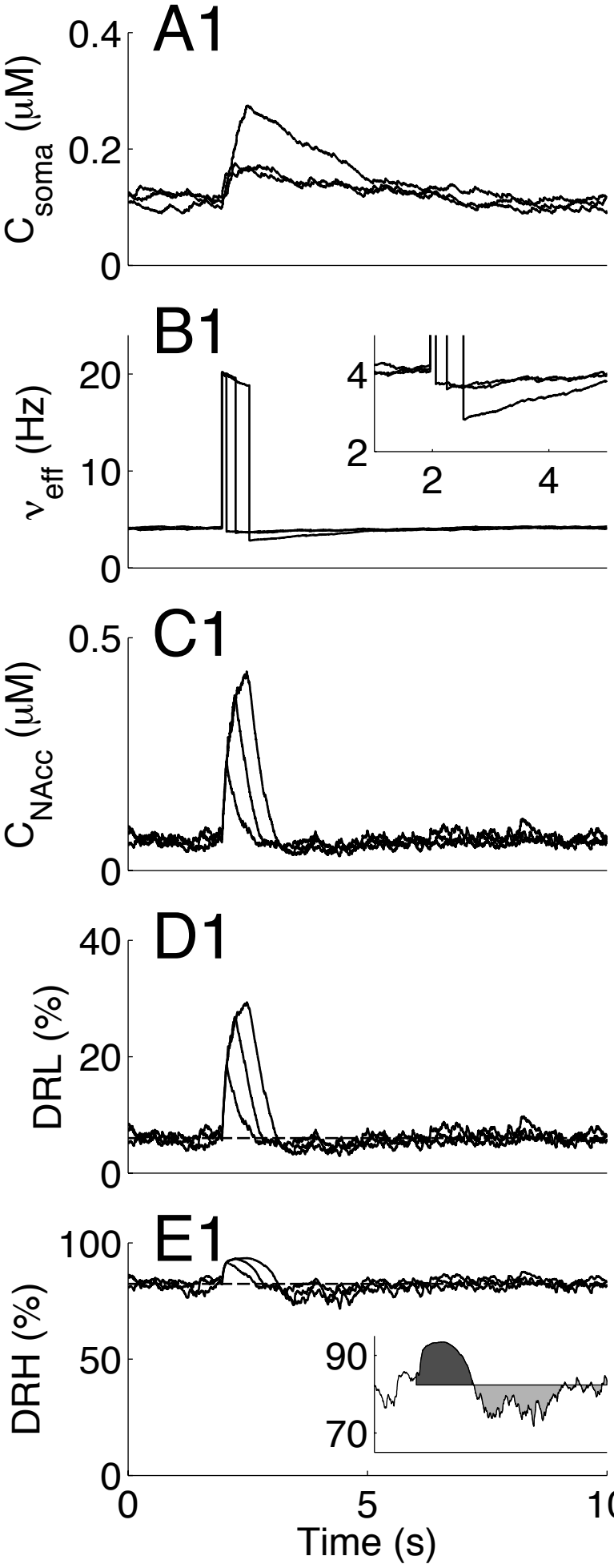
A1
0.4
0.2
0
C_{soma} (μM)

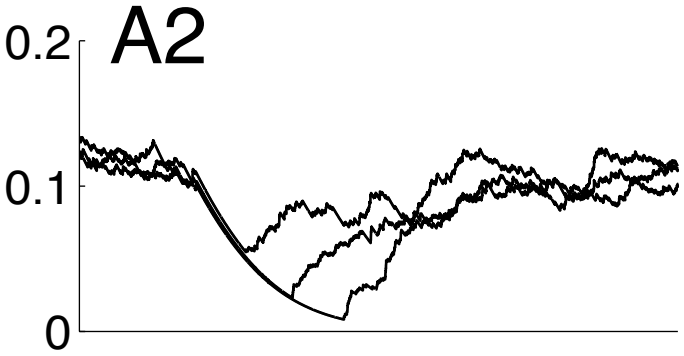
A2
0.2
0.1
0

B1
20
10
0
ν_{eff} (Hz)
4
2
2
4

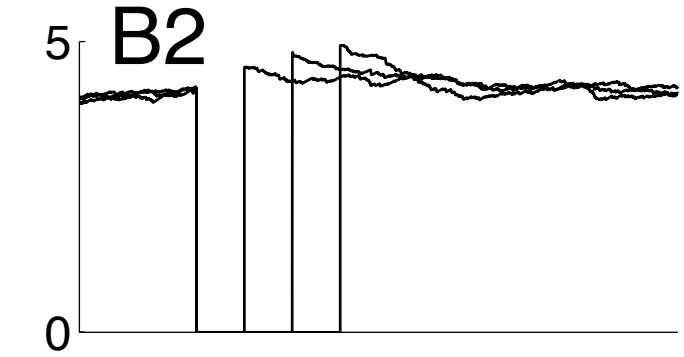
B2
5
0

C1
0.5
0
C_{NAcc} (μM)

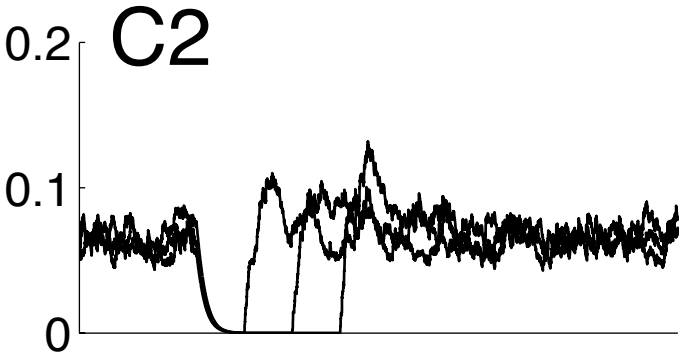
C2
0.2
0.1
0

D1
40
20
0
DRL (%)

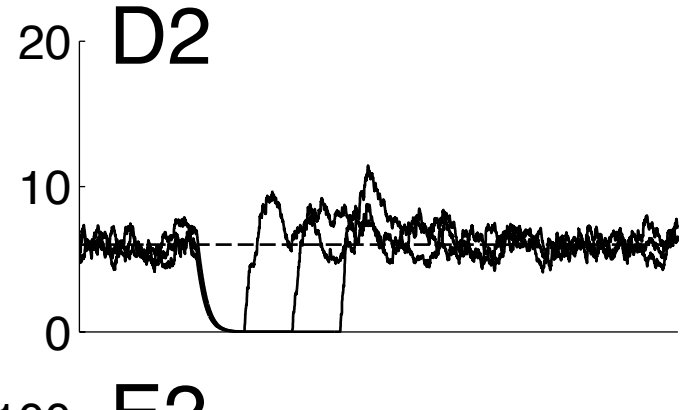
D2
20
10
0

E1
100
50
0
DRH (%)
90
70
0
5
10
Time (s)

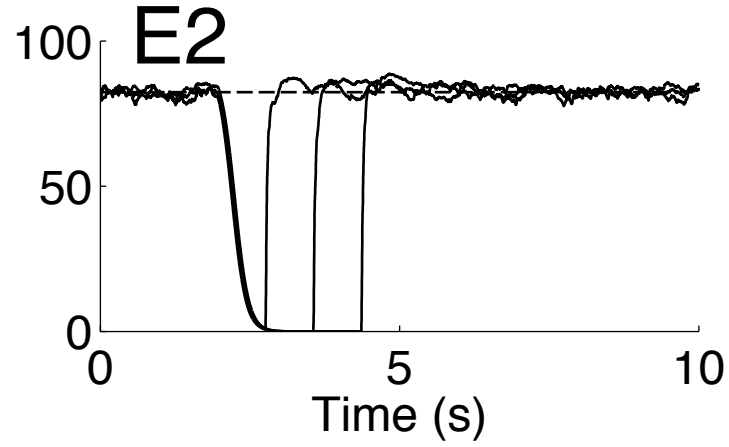
E2
100
50
0
0
5
10
Time (s)

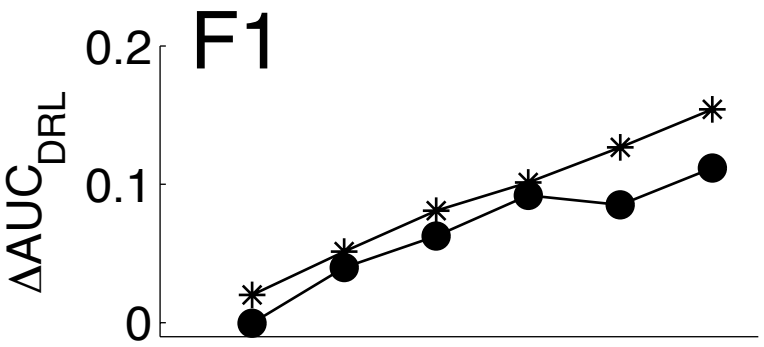
F1
0.2
0.1
0
ΔAUC_{DRL}

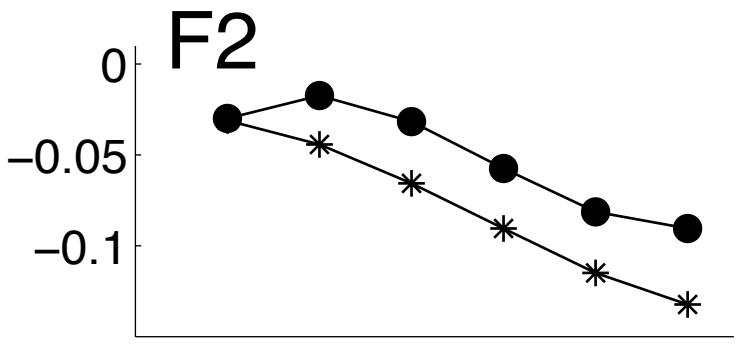
F2
0
−0.05
−0.1

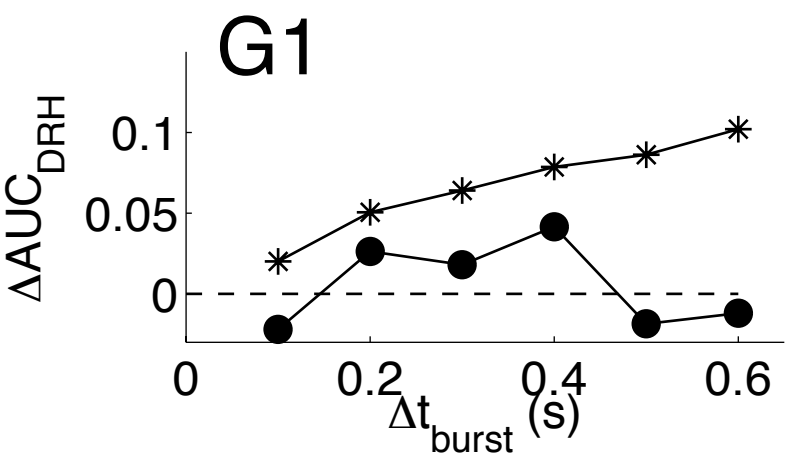
G1
0.1
0.05
0
ΔAUC_{DRH}
0
0.2
0.4
0.6
Δt_{burst} (s)

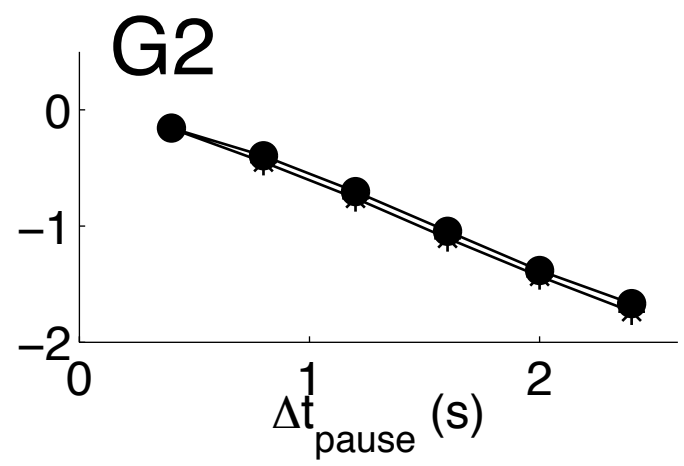
G2
0
−1
−2
0
1
2
Δt_{pause} (s)

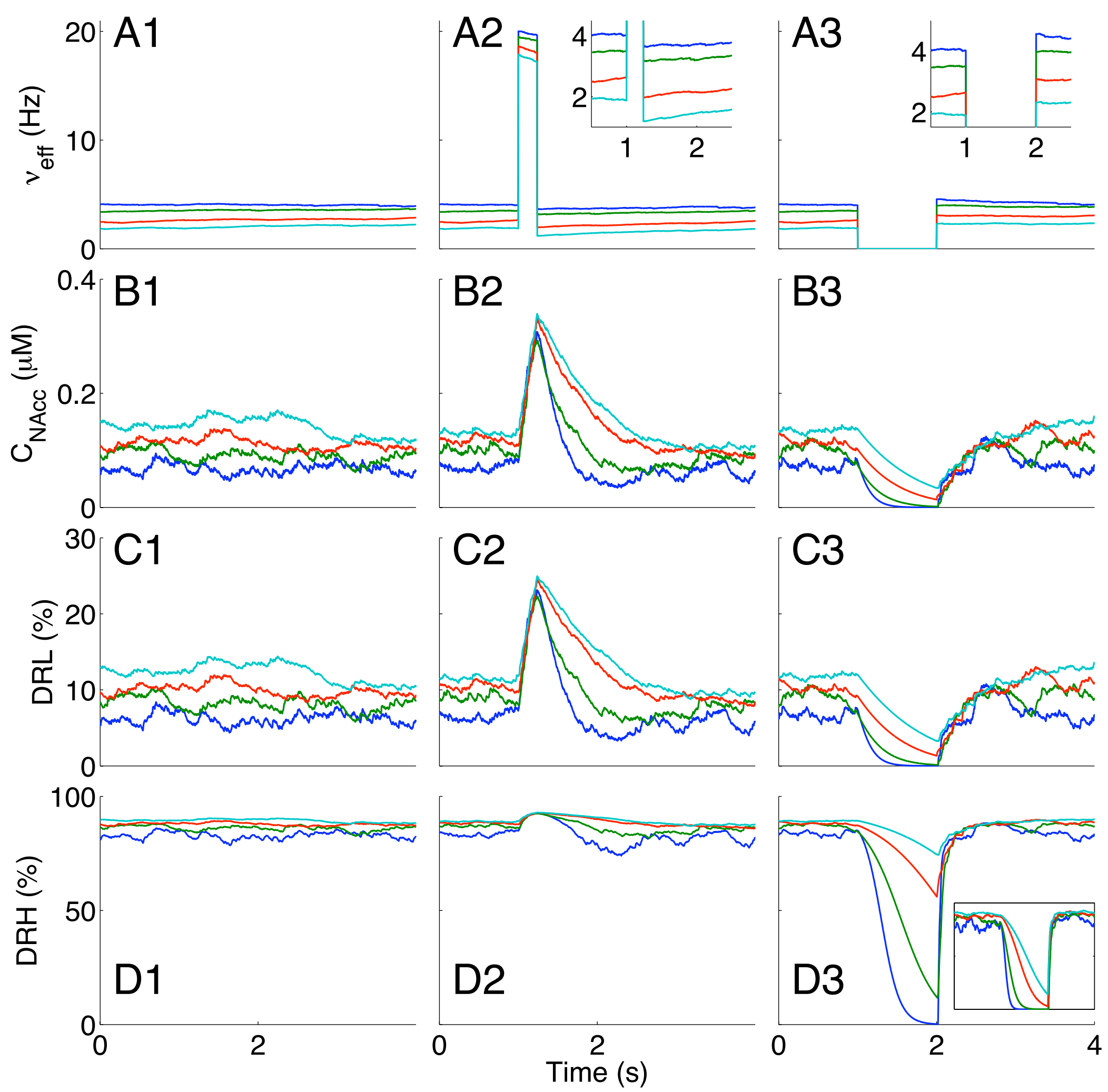
A1
A2
A3
B1
B2
B3
C1
C2
C3
D1
D2
D3
E1
E2
E3
ν_{eff} (Hz)
C_{NAcc} (µM)
DRL (%)
DRH (%)
Time (s)
inh./ctrl.
ΔAUC (s)
K_{app} (µM)